Article

Experimental evolution of magnetite nanoparticle resistance in *Escherichia coli.*

Akamu J. Ewunkem[1], LaShunta Rodgers[2], Daisha Campbell[3], Constance Staley[4], Kiran Subedi[5], Sada Boyd[6], and   Joseph L. Graves Jr[7,*]

[1]Department of Nanoscience, University of North Carolina at Greensboro, judeakamu@gmail.com

[2]Department of Biology University of North Carolina at Greensboro, Lmrodger2@gmail.com

[3]Department of Chemical, Biological, and Bioengineering, North Carolina A&T State. University, dmcampb2@gmail.com.

[4]Department of Chemistry, Bennett College, cbstaley26@gmail.com.

[5]College of Agricultural and Environmental Sciences (CAES), North Carolina A&T State University, ksubedi@ncat.edu.

[6]Department of Ecology and Evolutionary Biology, University of California, Los Angeles, smboyd@g.ucla.edu

[7]Department of Biology, North Carolina A&T State University, gravesjl@ncat.edu

 * Correspondence: gravesjl@ncat.edu; Tel.: 01-336-285-2858.

Abstract: Experimental evolution was utilized to produce 5 magnetite nanoparticle-resistant (FeNP$_{1-5}$) populations of *Escherichia coli*. The control populations were not exposed to magnetite nanoparticles. The 24-hour growth of these replicates was evaluated in the presence of increasing concentrations magnetite NPs as well as other ionic metals (gallium III, iron II, iron III, silver I) and antibiotics (ampicillin, chloramphenicol, rifampicin, sulfanilamide, tetracycline). Scanning electron microscope was utilized to determine cell size and shape in response to magnetite nanoparticle selection. Whole genome sequencing was carried out to determine if any genomic changes that resulted from magnetite nanoparticle resistance. After 25 days of selection magnetite resistance was evident in the FeNP treatment. The FeNP populations also showed a highly significantly (p < 0.0001) greater 24-growth as measured by optical density in metals (Fe (II), Fe (III), Ga (III), Ag and Cu II); as well as antibiotics (ampicillin, chloramphenicol, rifampicin, sulfanilamide, and tetracycline). The FeNP resistant populations also showed a significantly greater cell length compared to controls (p < 0.001). Genomic analysis of FeNP identified both polymorphisms and hard selective sweeps in the RNA polymerase genes *rpoA, rpoB*, and *rpoC*. Collectively, our results show that *E. coli* can rapidly evolve resistance to magnetite nanoparticles and that this result is correlated resistances to other metals and antibiotics. There were also changes in cell morphology resulting from adaptation to magnetite NPs. Thus, the various applications of magnetite nanoparticles could result in unanticipated changes in resistance to both metal and antibiotics.

Keywords: *Escherichia coli*, magnetite nanoparticles, metals, antibiotics, genomics, pleiotropy, cell morphology.

1. Introduction

Both ionic and nanoparticle iron have been proposed as a method to control multidrug resistant (MDR) bacteria [1—3]. This idea may seem contradictory in that all organisms require iron as an essential micronutrient. It often serves as an enzymatic co-factor, and therefore its intracellular concentration must be tightly regulated in order to maintain cell viability [4].   Iron is one of the most important micronutrients as it fulfills many biological roles [5]. Iron containing proteins (heme-proteins, iron-sulfur cluster proteins, and di-iron and mononuclear enzymes) play roles in nitrogen fixation, metabolism and serve as electron carriers for respiration [6]. However, despite its critical role in bacterial metabolism, acquiring iron is the greatest challenge for bacterial growth [4, 7]. Therefore, iron deficiency is one of the most common nutritional stress especially in aquatic environments [8]. The fundamental requirement for iron plays a crucial role in microbial pathogenesis, thus many organisms utilize iron sequestration as a defense against infection [9, 10].

Yet despite iron being an essential metal, it can also be extremely toxic under aerobic conditions [11]. There are multiple mechanisms of excess iron toxicity (see Table 1).   For this reason, iron homeostasis is tightly regulated.   Such tight regulation associated with the bacterial requirement to acquire iron from its environment can potentially be used as an evolutionary trap.   Evolutionary traps are defined as a situation in which an organism prefers resources that reduces its fitness [12]. Thus, in an environment where iron is present in excess we can ask the question whether bacteria have the capacity to control either the uptake, storage, or efflux of iron at rates sufficient to avoid toxicity?   Alternatively, it is important to ask: can and how do bacteria evolve resistance to excess iron? In addition, if they can what correlated traits will result from the adaptation?   We have already answered some of these questions in a series of experiments utilizing ionic iron II, iron III, and the iron analog gallium III [13—15]. These studies utilized experimental evolution and examined mechanisms of iron and gallium resistance through the evaluation of phenotypic and genomic changes in *E. coli* K-12 MG1655.   We found that this strain of *E. coli* was capable of evolving resistance to excess iron and gallium primarily through changes in the uptake of iron (or gallium). Our results suggested that *E. coli* K-12 could respond to excess iron by both physiological acclimation and evolutionary adaptation [13]. This was manifested by both patterns of genomic and gene expression changes exhibited in the iron (II), iron (III), and Gallium (III)-resistant populations compared to their ancestors and controls (grown in the absence of excess iron or gallium).

Table 1. Mechanisms of excess iron and silver toxicity: Mechanisms of cellular damage are listed resulting from excess iron toxicity.   As these systems are common to virtually all bacteria there is a strong potential that resistance mechanisms might be conserved across wide varieties of taxa.

Mechanism	Fe
Reactive oxygen species	+
Disruption of transcription/translation	+
Damage to cell wall/membrane	+
Interfering with respiration	+
Release of cellular components	+
Binding to thiol groups	+

In this study we examine whether experimental evolution against spherical magnetite nanoparticles (FeNPs) will result in similar outcomes as those observed resulting from selection for ionic iron (II, III) resistance.   Nanoparticles (NPs) are particles between 1 and 100 nanometers in size [16]. NPs are broadly classified into various categories depending on their morphology, size, and chemical properties [17, 18]. Metallic ferrous nanoparticles are one of the most studied nanomaterials against multidrug-resistant bacteria [19]. The three most common naturally occurring forms of metallic ferrous NPs are hematite (α-Fe_2O_3), maghemite (γ-Fe_2O_3) and magnetite (Fe_3O_4 or $FeO.Fe_2O_3$).   Magnetite is a black iron oxide, commonly called Hercules stone and possesses the strongest magnetic behavior [20]. Magnetite is considered as a charge frustrated iron oxide due to the distribution of both iron (II) and (III) in crystallographic sublattice sites [21].

Magnetite NP's exist in nature and engineered FeNPs are widely used in a range of applications due to their advanced optical properties [18]. FeNPs can be used to determine oxygen concentrations [22—24]. FeNPs are involved in orientation, navigation, and iron metabolism in prokaryotic and eukaryotic cells [22, 25].   FeNPs are extensively used for applications in biomedicine and bioanalytics [26—31]. FeNPs are also now use for antimicrobial applications due to their very small in size and high surface area to volume [32, 33]. FeNPs disseminate ionic iron II and iron III species with low toxicity to eukaryotic host cells minimizing undesirable side effects [29, 34—36]. The antibacterial properties of the FeNPs have been tested against *Bacillus cereus, Escherichia coli*, and *Candida albicans, Staphylococcus aureus* and *Pseudomonas aeruginosa* and *Serratia marcescens* [34, 37].

However, none of these studies considered the possibility that bacteria could evolve resistance to FeNPs. Therefore, it is of paramount importance to describe mechanisms by which bacteria can become resistant to magnetite NP's and determine if resistance to magnetite nanoparticles confers resistance to ionic metals and antibiotics in order to fill gaps in our knowledge.   In this study, we investigated how rapidly bacteria can evolve resistance to FeNPs; and evaluated the nature of the genomic changes responsible for that resistance. In addition, we wanted to determine is magnetite resistance conferred correlated resistances to ionic metals and antibiotics. Finally, we wished to determine the similarity of phenotypic and genomic changed due to magnetite to those produced by ionic iron (II) and (III) resistance.

2. Materials and Methods

Bacterial strains

E. coli MG1655 (ATCC #47076) was used in this study because it does not have plasmids and its circular chromosome is composed of 4,641,652 nucleotides (GenBank: NC_000913.3; Riley et al. 2006). All of our previous studies of ionic and nanoparticle resistance have used this strain [13—15]. This strain is the ancestor of all the selection treatments (FeNP and Controls) evaluated in this study.

Evolution experiment

E. coli MG1655 (ATCC #47076) was routinely cultured in Davis Minimal Broth (DMB, Difco™Sparks, MD) with 1 gram per liter of Dextrose (Dextrose, Fisher Scientific, Fair Lawn, NJ) as the sole carbon source. The broth was supplemented with thiamine hydrochloride 10 μL in a final volume of 10 ml of total culture maintained in 50 ml Erlenmeyer flasks. The Bacteria were incubated at 37 °C in broth at 150 rpm overnight and propagated by transferring 0.1 ml into 9.9 ml of fresh sterile DMB daily. We established 5 populations within the magnetite NP-selection treatment.   Each population was founded from a unique colony resulting from serial

dilution after 24-hour growth of the ancestral *E. coli* K-12 MG1655 sample.   These replicates were exposed daily to 750mg/L 20 nm spherical PVP-coated FeNPs (designated $FeNP_{1-5}$).   The magnetite nanoparticles were obtained from Nanocomposix (San Diego, CA).   The concentrations utilized to initiate the selection experiment were determined by minimum inhibitory assay (MIC, described below). The controls (designated C_1–C_5) were cultured in standard DMB medium without the addition of magnetite nanoparticles.

Determination of Minimal inhibitory concentration (MIC) of Magnetite NPs

Minimum inhibitory concentration (MIC) values were assessed by measuring the growth rates of *E. coli* K-12 MG1655 by estimating their optical density at 625 nm (OD_{625}). OD_{625} is an absorbance measurement at a wavelength of 625 nm in an accuSkan Go spectrophotometer (Fisher Scientific, USA). MIC is defined as the lowest concentration of an antimicrobial that will inhibit the visible growth by ~90% after 24 h of incubation at 37°C compared with a growth control [38]. These values were determined by broth dilutions in a 96-well microtiter plate format consisting of ten concentrations (0-5000 mg/L) in triplicates of magnetite NPs. The plates were incubated at 37°C and agitated at 600 rpm in an I2500 Series incubator shaker (New Brunswick Scientific, USA). The OD_{625} was measured after incubation at 37°C for 24 h. The MIC was determined to be 1000.0 mg/L. A sub-MIC value (750 mg/L) was chosen to initiate the selection experiment.   This value allowed for the initial growth of cultures without causing their extinction.

Phenotypic assays: 24-hour growth

To determine if magnetite NP resistance confers correlated resistances to other metals and antibiotics, assays were conducted to assess 24-hour growth to different concentrations of ionic forms of metals [Ag (I), Fe (II), Fe (III), Ga (III)] and the antibiotics [ampicillin, chloramphenicol, rifampicin, tetracycline].   These heavy metals and antibiotics and are known to have different mechanisms of action. The ancestral strain was grown for 24 hours in DMB broth and serial dilution was used to pick 5 independent colonies.   These in turn were used to found replicates grown for 24 hours and placed into the various phenotypic assays. The FeNP and control populations were sampled at 25 days in their various media for use in these assays. Bacterial growth was assessed by measuring at turbidity at 625 nm for hours 0 and 24h, using a 98-well plate format accuSkan Go spectrophotometer (Fisher Scientific, USA) using clear polyester 98-well plates

Genomic analysis

Whole genome resequencing was utilized to identify genomic variants associated with FeNP and control populations. DNA was extracted from each replicate population at 25 days of selection in magnetite NP using EZNA Bacterial DNA kit (OMEGA) following manufacturer instruction. DNA concentrations were determined fluorometrically using the QuantiFluor® ONE dsDNA System (Promega Corporation, Madison, WI, USA) on a Quantus® fluorometer (Promega Corporation). Measurements were performed according to the manufacturer's recommendations. Genomic libraries were prepared using the standard protocol as described in the manufacturer's instructions (Illumina, Nextera DNA Flex Library Prep Reference Guide). All the reagents used are included in the Nextera DNA Flex kit (Illumina, cat. Nos. 20,018,704, 20,018,705).
The quality of the final library was verified using D1000 Screen Tape (Agilent Technologies, CA, USA) following the manufacturer's instruction. Library concentration was measured using the fluorometric

quantification using the dsDNA binding dye as previously described and diluted 12pM with Resuspension Buffer. The pooled libraries were then run on an Illumina MiSeq (Illumina, San Diego, CA) using the MiSeq v3 reagent kit.   The depth of coverage of the sequencing runs ranged from ~20X to ~80X, with most exceeding 40X coverage.   The SRA accession number for sequencing data is PRJNA694183 (FeNP-resistant, $FeNP_{1-5}$_D28 and controls, C_{1-5}_D28).

Sequence alignment and variant calling from the samples was achieved by use of the breseq 0.30.0 pipeline set to polymorphism mode (-p) and default parameters [39].   The pipeline makes use of three types of evidence to predict mutations, read alignments (RA), missing coverage (MC), and new junctions (JC) [40]. Reads that shows a distinction between the sample and the reference genome that cannot be resolved to describe precise genetic changes are considered "unassigned" and would not be described nor interpreted. Finally, we report here only genomic variants that were not present in the ancestral population.   Variants in our ancestral founding populations that differ from the *E. coli* K-12 MG1655 reference genome are reported in our previous studies [41, 42].

Preparation of cells for scanning election microscope

Scanning electron microscopy (SEM) is widely used to measure changes in morphology of bacteria [43]. After resistance to FeNPs was observed (at 25d of selection) the outer morphology of the bacterial cells was examined using a Carl Zeiss Auriga-BU FIB FESEM (FESEM) (Carl Zeiss, Jona, Germany). Briefly, bacterial samples from each population were placed on cover slips after 10 minutes of incubation at room temperature, the samples were gently removed. Thereafter, the bacteria were fixed with Karnovsky fixative and incubated at 4°C overnight. Following incubation, the samples were dehydrated with graded ethanol and then air-dried. The samples were then sputtered to avoid charging in the microscope. The images were acquired at a working distance of 7mm and an accelerating voltage of 3kV.

Inductively Coupled Plasma Optical Emission Spectrometry (ICP-OES) Analysis

The amount of ionic materials released into solution by metallic nanoparticles vary considerably depending upon conditions of the medium [44]. For this reason, an ICP-OES study was performed to determine or define the sublethal concentration of iron in samples utilized for MIC assays at 12 and 24h. Operating conditions are shown in Appendix A Table A1. Each sample was carefully pipetted and transferred to digestion tubes followed by the addition of concentrated nitric acid (67-70) % purchased from Fisher Scientific. After allowing for a 15-minute pre-digestion procedure, the samples were digested in an automated sequential microwave digester, MARS 5 (CEM Microwave Technology Ltd., North Carolina, USA).   The final product was a clean, transparent aqueous solution which was further diluted to a volume of 50ml using double DI water. The concentration of acid in the final solution was <5%.   A set of matrix matched standards were prepared to set up a calibration curve. All the samples were analyzed by using Optima 8300 (PerkinElmer, Inc. Shelton, CT, USA) in axial mode.

Statistical Analysis

Statistical analysis of the effect of selection regime and concentration (and their interaction) for all 24-hour growth data was performed via General Linear Model utilizing SPSS version 26 (SPSS Inc, Armonk, NY, USA). All graphs in this paper were made via Prism 9 software.   Finally, the phenotypic data from these studies will be submitted into DRYAD (https://datadryad.org/) upon acceptance of this manuscript for publication.

3. Results

Escherichia coli can rapidly evolve resistance to stressful levels of magnetite NPs:

The FeNP populations showed statistically significantly greater 24-hour growth compared to the controls with increasing concentration in every substance tested as tested by general linear model that examined the effect of population, concentration of substance, and their interaction.   The F and p values for all phenotypic assays (antibiotics and metals) are given in Table 2a. The controls showed statistically significantly greater growth compared to the ancestors for all substances tested except for ampicillin and rifampicin. As the comparison for magnetite, silver (I), and chloramphenicol was not as clear, general linear model results are reported for these substances in Table 2b. The 24-hour growth after 25 days of selection in magnetite showed that FeNP populations exhibited a highly significantly superior growth compared to the control and ancestral populations across all concentration of magnetite NP (Figure 1).   The FeNP populations show statistically significant greater growth than either the controls or ancestors from 250—1750 mg/L. The 24-hour growth of the FeNP population increased across this range while that of the control and ancestors decreased until there was very little growth from 500—1750 mg/L.   There was no observable growth for any population at 2500 mg/L (data not shown).

Table 2a. General Linear Model Results for Phenotypic assays, FeNP v. Control

Substance	Pop. Effect (F, p)	Conc. Effect (F, p)	Interaction (F, p)
magnetite	383.9, 0.001	42.5, 0.001	25.9, 0.001
ampicillin	283.1, 0.001	17.1, 0.001	16.7, 0.001
chloramphenicol	71.1, 0.001	114.6, 0.001	7.9, 0.001
rifampicin	1,285.1, 0.001	16.3, 0.001	16.5, 0.001
tetracycline	62.9, 0.001	12.6, 0.001	5.7, 0.001
iron (II)	18.6, 0.001	88.0, 0.001	1.7, 0.116
iron (III)	42.9, 0.001	77.4, 0.001	2.7, 0.011
gallium (III)	29.8, 0.001	111.8, 0.001	1.2, 0.278
silver (I)	7.1, 0.009	15.8, 0.001	2.3, 0.029

Table 2b. General Linear Model Results for Phenotypic assays, Control v. Ancestor

Substance	Pop. Effect (F, p)	Conc. Effect (F, p)	Interaction (F, p)
magnetite	9.5, 0.003	22.7, 0.001	12.8, 0.001

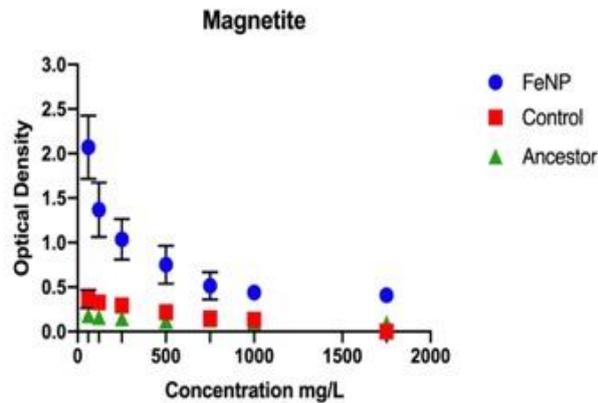| chloramphenicol | 159.1, 0.001 | 25.7, 0.001 | 22.6, 0.001 |
| silver (I) | 243.1, 0.001 | 10.4, 0.001 | 15.6, 0.001 |

Figure 1: The mean and SE of 24h-hour growth for FeNP, Control, and Ancestral populations in increasing concentration of Magnetite NPs are shown. There was no observable growth at 2,000 mg/L magnetite for the FeNP population.

Metal resistance

Measurement of 24-hr growth in excess metal (iron (II), iron (III), gallium (III), silver (I)) was accessed for the FeNP, control, and ancestral populations at 25 days of evolution (Figures 2a-d).   The FeNP showed highly statistically greater 24-hour growth across concentration compared to the controls which were greater than the ancestors in magnetite, iron (II), iron (III), gallium (III), and silver (I) Table 2a.   Iron (II) and iron (III) are of particular interest to this study because in solution, magnetite nanoparticles release both iron (II) and iron (III) ions into the medium.   Measurements by ICP-OES determined how much of each of these species was released relative to the measured mass of that species added to DMB medium (Appendix A Table A2, figures A1—A3).   These figures show that the actual amount of iron entering into solution was always considerably less than the measured amounts initially added to the medium.   The iron contents in these solutions were in the following order magnetite NPs > iron (III) > iron (II). The method presented was assessed by utilizing aliquots and dilutions of magnetite NPs, iron (II), and iron (III). The emission line used for the quantification of Fe (II) was 259.9 nm. Results showed high precision with the relative standard deviation (RSD) values for most of the samples < 2%.   The plotted calibration curve was linear with a R^2 value > 0.999.

The controls also showed statistically greater growth in all metals across concentration compared to the ancestor.
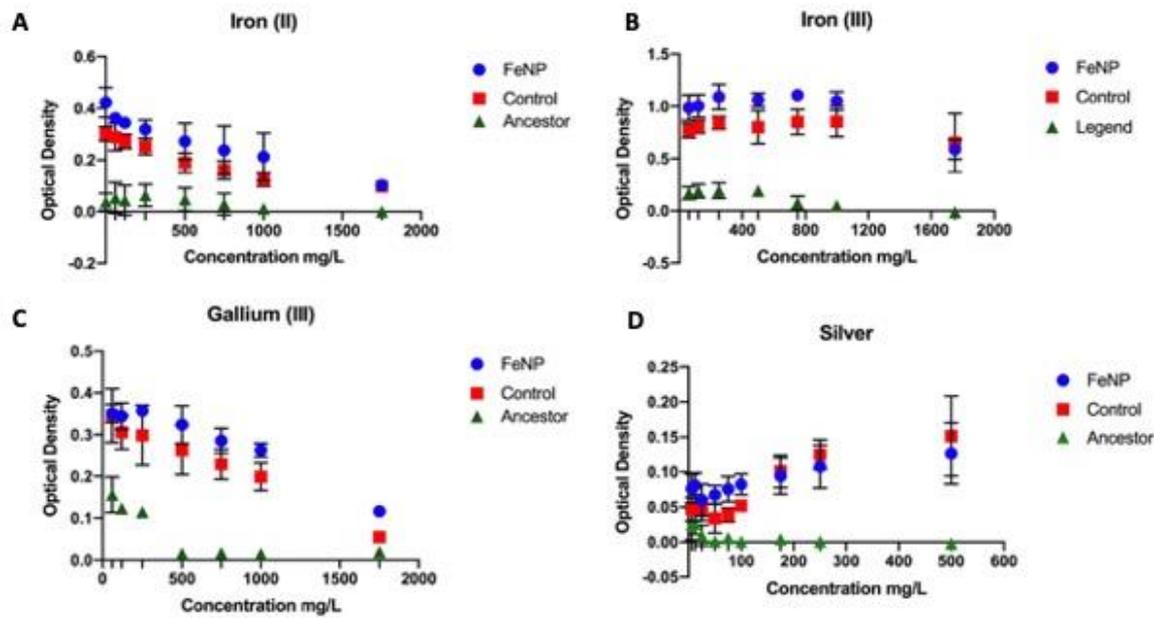
The mean and SE of 24h-hour growth for FeNP, Control, and Ancestral populations in increasing concentration of metals are shown. The FeNP populations showed superior growth compared to controls for iron (II, III) and gallium (III) from 6—1750 mg/l. For silver superiority was shown from 6—100 mg/L. The ancestor showed inferior growth to the FeNPs and controls at all concentrations.

Antibiotic resistance

The FeNP populations, controls, and ancestors were evaluated at 25 days of evolution for general antibiotic resistance (Fig. 3a-d).   FeNP populations showed superior growth in ampicillin and rifampicin compared to controls and the ancestral population at all concentrations (Figure 3a—d).   FeNP populations showed significantly greater growth compared to the controls and ancestors for variable ranges in (chloramphenicol (6—12 mg/L); tetracycline (75—250 mg/L). The controls showed superior growth compared to the ancestral population in chloramphenicol (6—50 mg/l); and tetracycline 6—175 mg/L.   All populations showed a reduction in growth with increasing concentration of antibiotics. All comparisons between FeNP and controls in antibiotics showed a significant interaction effect, indicating that the functional response to the antibiotic differed between these populations (Table 2a). Similarly, in the comparison of the controls to the ancestors, significant interaction effects were also seen for all antibiotics (Table 2b).
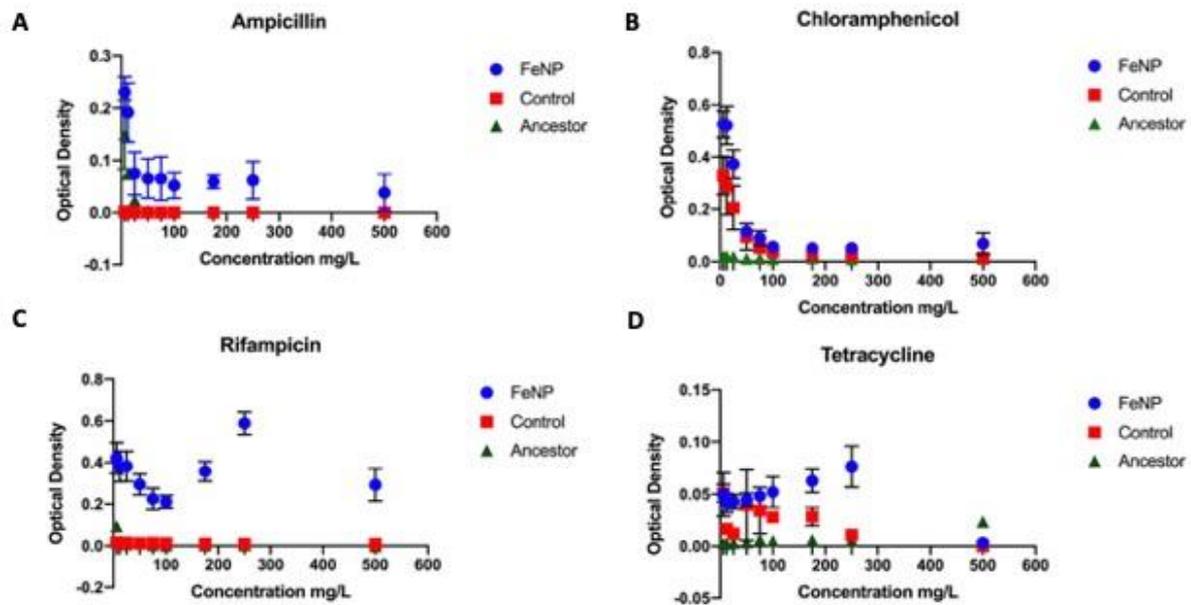
The mean and SE of 24h-hour growth for FeNP, Control, and Ancestral populations in increasing concentration of antibiotics are shown. The FeNP populations showed superior growth compared to controls for all antibiotics. The controls were equivalent to the ancestors in ampicillin and rifampicin.

Cell Length and width Distribution

The size distribution of FeNP, control, and ancestral populations after 25 days of selection were determined by scanning electron microscopy (SEM).   FeNP populations showed a significant increased cell length (2,159.4 +/- 15.3 versus 1,310.4 +/- 24.1 nm) and width (582.0 +/- 1.63 versus 471.8 +/- 16.2 nm) compared to the control and ancestral populations (F = 395.9, p < 0.000; Figure 4).   There was no replicate effect for length (F = 0.255, p < 0.906); but there was significant population by replication effect (F = 4.32, p < 0.002).   The controls were also slightly longer in length compared to the ancestral population 1,310.4 +/- 24.1 versus 1,248 +/-14.4 nm; F = 4.5, p < 0.034.). There was a significant replicate effect and population by replicate interaction (F = 6.7, p < 0.001 and F = 2.5, p < 0.041 respectively).   The population effect on cell width was F = 79.4, p < 0.001; replicate effect was F = 8.6, p < 0.001; with an interaction for population and replicate at F = 8.6, p < 0.001 for the comparison of the FeNP with the controls.   The mean cell width for the ancestors was not significantly different from the controls (F = 0.493, p < 0.483). There was significant variation within the ancestral population replicates for cell width (F = 8.1, p < 0.001); as well as significant interaction between population and replicates (F = 6.2, p < 0.001).
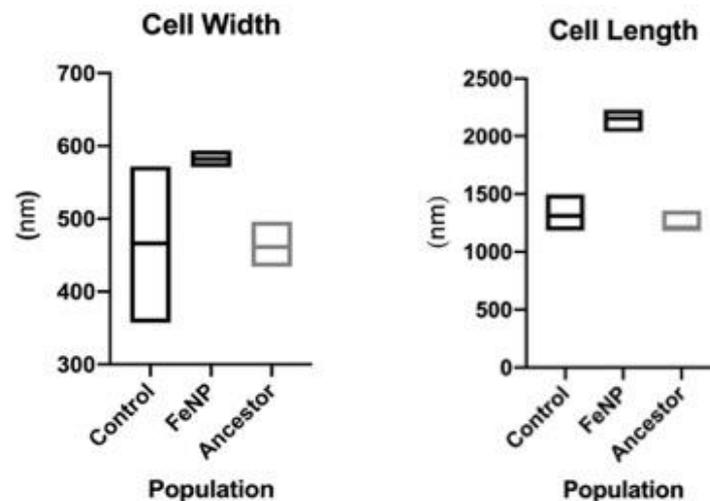
Bacteria cell width and length distribution. Box plots of *E. coli* MG1655 mean cell width and length for FeNP compared to controls and ancestors is shown. The sample size was N = 20 cells per replicate population measures in the FeNP and control populations for a total of 100 cells per selection treatment. Sample size for ancestors was 15 for each replicate, for a total of 75 cells.

Whole Genome

The genomic variants found in the FeNP are listed in Table 3a—c.   Descriptions of these genes are given in Table 4a—c.   The genomic variants for the controls are provided in Appendix B Tables B1, B2. The controls showed no hard selective sweeps.   Also, genomic variants for the ancestral population are not reported here as these are given in our prior research [41, 42].   The ancestral variants were filtered out of all variant calls in the FeNP and Control populations. At 25 days three of the five FeNP replicates (FeNP$_1$, FeNP$_2$, & FeNP$_5$) displayed a hard selective sweep for non-synonymous (NS) substitutions in the RNA polymerase subunit β' (*rpoC*) gene.   Significant polymorphisms in RNA polymerase subunit α (*rpoA*) were observed in FeNP$_3$ and FeNP$_5$ (f = 0.503, 0.665 respectively).   FeNP$_4$ was the only population displaying no hard selective sweeps but had significant polymorphisms in the flagellar hook protein (*flgE*) and NADH: ubiquinone oxidoreductase, chain G (*nuoG*) genes (f = 0.295, 0.439 respectively).

Significant polymorphisms (f > 0.250) were observed in all replicates (Table 3b).   FeNP$_1$ showed NS polymorphisms in porphyrinogen oxidase, cytoplasmic (*yfeX*), and putative metal dependent hydrolase (*ygjP*). FeNP$_2$ had NS polymorphisms in hydroxyacylgluthione hydrolase (*gloB*) and a synonymous substitution in the glutamate/aspartate: proton symporter (*gltP*).   Synonymous substitutions may result from linkage to a NS beneficial mutation, or they can result from favorable selection due to codon bias.   FeNP$_3$ had NS polymorphisms in RNA polymerase α subunit (*rpoA*) and a synonymous variant in chromate reductase, Class I, flavoprotein (*chrR*). FeNP$_4$ in flagellar hook protein (*flgE*) and NADH ubiquinone oxidoreductase, chain G (*nuoG*). Finally, FeNP$_5$ also showed a significant NS polymorphism in RNA polymerase, α subunit (*rpoA*). Minor polymorphisms are listed in Table 3c. The controls displayed significant NS polymorphisms in RNA polymerase subunits β and β'. These are often associated with adaptation to minimal medium such as

DMB. The *rpoB* H526Y variant has been repeatability observed arising in our control populations in several of our past studies [41,42.]

Table 3a: Selective Sweeps in FeNP-resistant populations at day 25

Gene	Mutation	Annotation	FeNp1	FeNp2	FeNp3	FeNp4	FeNp5
rpoC →	A→T	D410V (GAT→GTT)	0.000	0.000	0.000	0.000	1.000
rpoC →	A→G	D622G (GAC→GGC)	1.000	1.000	0.000	0.000	0.000

Table 3b: Significant polymorphisms in FeNP-resistant populations at day 25

Gene	Mutation	Annotation	FeNp1	FeNp2	FeNp3	FeNp4	FeNp5
gloB ←	T→A	E239V (GAG→GTG)	0.000	0.277	0.000	0.000	0.000
flgE →	C→T	A28A (GCC→GCT)	0.000	0.000	0.000	0.295	0.000
nuoG ←	C→T	G792S (GGT→AGT)	0.000	0.000	0.000	0.439	0.000
yfeX ←	G→T	L263M (CTG→ATG)	0.251	0.000	0.000	0.000	0.000
ygjP →	A→G	Q17R (CAG→CGG)	0.270	0.000	0.000	0.000	0.000
rng ←	T→A	H76L (CAC→CTC)	0.000	0.000	0.000	0.250	0.000
rpoA ←	C→A	D199Y (GAC→TAC)	0.000	0.000	0.503	0.000	0.000
rpoA ←	G→A	R191C (CGT→TGT)	0.000	0.000	0.000	0.000	0.665
chrR →	G→A	P32P (CCG→CCA)	0.000	0.000	0.258	0.000	0.000
gltP →	A→G	G250G (GGA→GGG)	0.000	0.302	0.000	0.000	0.000

Table 3c: Minor polymorphisms in FeNP-resistant populations at day 25

Gene	Mutation	Annotation	FeNp1	FeNp2	FeNp3	FeNp4	FeNp5
yagL ←	T→A	E93V (GAG→GTG)	0.000	0.165	0.000	0.000	0.000
gapC ←	C→T	pseudo-gene (254/750 nt)	0.000	0.000	0.134	0.000	0.000
lsrD →	A→T	N258I (AAT→ATT)	0.000	0.000	0.159	0.000	0.000
pta →	C→T	R669C (CGT→TGT)	0.000	0.207	0.000	0.000	0.000
intS →	G→A	G77S (GGC→AGC)	0.000	0.175	0.000	0.000	0.000
yraJ →	A→G	K85E (AAG→GAG)	0.154	0.000	0.000	0.000	0.000
prmA/dusB	A→T	intergenic (+317/-12)	0.000	0.000	0.000	0.000	0.209
hdeB ←	A→T	N31K (AAT→AAA)	0.000	0.000	0.000	0.000	0.155
viaA ←	T→A	E153V (GAA→GTA)	0.000	0.000	0.161	0.000	0.000
frwA ←	C→T	E363E (GAG→GAA)	0.000	0.000	0.183	0.000	0.000
treR ←	C→T	P275P (CCG→CCA)	0.000	0.000	0.000	0.000	0.111
sgcX ←	C→A	Q155H (CAG→CAT)	0.152	0.000	0.000	0.000	0.000

Table 4a: Position and Description of Selective Sweeps in FeNP-resistant populations at day 25

Gene	Position	Description
rpoC →	4,186,578 & 4,187,214	RNA polymerase, beta prime subunit

Table 4b: Position and Description of Significant polymorphisms in FeNP-resistant populations at day 28

Gene	Position	Description
gloB ←	234,067	hydroxyacylglutathione hydrolase
flgE →	1,132,657	flagellar hook protein
nuoG ←	2397792	NADH: ubiquinone oxidoreductase, chain G
yfeX ←	2,549,759	porphyrinogen oxidase, cytoplasmic
ygjP →	3,236,009	putative metal dependent hydrolase
rng ←	3,397,569	ribonuclease G
rpoA ←	3,440,435 & 3,440,459	RNA polymerase, alpha subunit
chrR →	3,894,747	chromate reductase, Class I, flavoprotein
gltP →	4,295,230	glutamate/aspartate: proton symporter

Table 3c: Position and Description of Minor polymorphisms in FeNP-resistant populations at day 25

Gene	Position	Description
yagL ←	293,641	CP4-6 prophage; DNA-binding protein
gapC ←	1,490,460	pseudogene, GAP dehydrogenase; 1.
lsrD →	1,604,819	autoinducer 2 import system permease protein
pta →	2416751	phosphate acetyltransferase
intS →	2,466,773	CPS-53 (KpLE1) prophage; putative prophage CPS-53 integrase
yraJ →	3,289,066	putative outer membrane protein
prmA/dusB	3,410,268	methyltransferase for 50S ribosomal subunit protein L11/ 2.
hdeB ←	3,656,200	acid-resistance protein
viaA ←	3,929,146	stimulator of RavA ATPase activity; 3.
frwA ←	4,141,133	putative PTS enzyme, Hpr component/enzyme I component/ 4.
treR ←	4,466,422	trehalose 6-phosphate-inducible trehalose regulon 5.
sgcX ←	4,531,187	putative endoglucanase with Zn-dependent exopeptidase domain

1. glyceraldehyde-3-phosphate dehydrogenase (second fragment).
2. tRNA-dihydrouridine synthase B
3. von Willebrand factor domain protein
4. enzyme IIA component
5. transcriptional repressor

4. Discussion

The study examined the potential for *E. coli* K-12 MG1655 to evolve magnetite nanoparticle resistance.   It also examined the genomics changes associated with magnetite nanoparticle resistance.

We demonstrated that by day 25 increased magnetite NP resistance was apparent in populations cultured in magnetite NPs (FeNP$_{1—5}$).   The FeNP replicates displayed highly statistically different increases (between 50—2 times greater) 24-hour growth across concentration in magnetite with a mean increase across concentration of 8.5 times.   They were highly statistically significantly higher in their capacity to grow in magnetite compared to the controls by similar margins.   The controls display adaptations to growth in DMB medium that are not seen in the ancestors.   As far as we know this is the first report of the experimental evolution of magnetite resistance in the literature.

Resistance to magnetite NPs also conferred greater fitness in increasing concentrations to ionic metals iron (II), iron (III), gallium (III), and silver. The FeNP populations showed highly statistically significantly greater resistance to all of these metals compared to controls and ancestors as well.   Similarly, FeNP populations showed significantly greater resistance to ampicillin, chloramphenicol, rifampicin, sulfanilamide and tetracycline compared to controls and ancestors.

One of the most striking results of this study was the shift in cell proportions in the FeNP populations compared to the controls and ancestors.   The FeNP populations increased in both their length and width compared to both.   As *E. coli* is a rod-shaped bacterium, a rough calculation of the increase in the cell area is given by multiplying its length and width. On average FeNP area = 1.25×10^6 nm^2; control = 6.17×10^5 nm^2; and ancestor = 5.76×10^5 nm^2.   This represents a 2.18-fold increase in cell area in the FeNP populations compared to their ancestor.   The magnitude of the cell size response suggests that this may be playing an important role in FeNP adaptation to metal and antibiotic toxicity.   On the primary mechanisms by which magnetite is known to impact bacteria is via ROS [45, Table 1].   Table 1).   There is evidence that larger cell size is correlated to ROS resistance.   A study of *Lactobacillus* species found that greater cell size was positively associated with resistance to ROS [46].   Another study of Mycobacterium isolates found that greater size variation was associated with antibiotic resistance [47]. In *E. coli* MG1655 stress is known to cause an increased cell length; this has also been observed in *M. tuberculosis* and *M. smegmatis* [48, 49].   Finally, it has been shown that increase in cell length is an adaptation associated with antibiotic resistance due to the synthesis of a modified nucleotide in response to stress (p) ppGpp [50—53].

Genetics analysis identified selective sweeps in RNA polymerase subunit β' (*rpoC*) in some replicates.   In addition, others displayed significant polymorphisms (f > 0.500) in RNA polymerase subunit α (*rpoA*).   As RNA polymerase is involved in putting together all the RNA in the cell, mutations in this protein are known to be widely pleiotropic and play major roles in relieving stress and increasing metabolic efficiency in *E. coli* [54, 55].   This may explain why the FeNP populations displayed superior growth compared to the control and ancestral populations in all the stresses applied to them in this study (magnetite, ionic metals, and antibiotics).

Despite the fact that the FeNP populations displayed an increase in growth in magnetite, iron (II), iron (III), and gallium (III, an iron III analog) we did not find selective sweeps of variants associated with iron resistance in our prior studies [14—16]. These included mutations in genes such *as fecA, fur, dnaK, murC, ptsP* and *ilvG*.   Magnetite contains both iron (II) and iron (III) and these are released in solution [1].   In this study the γ-magnetite particles were stabilized by a coating of tetramethylammonium hydroxide (CH$_3$)$_4$NOH.   In our study the magnetite nanoparticles were stabilized with PVP (polyvinylpyrrolidone). Coating agents used to improve the stability of   magnetite nanoparticles decrease the release of ionic Fe^{2+} and Fe^{3+} in the medium [56, 57].

Resistance to magnetite NP conferred resistance to all the antibiotics tested. These antibiotics have different modes of action due to the nature of their structures and degree of affinity to certain target sites within bacterial cells.   Ampicillin exerts bactericidal activity through inhibition of bacterial cell wall synthesis by binding to penicillin binding proteins (PBPs) and by inhibiting certain PBPs related to the activation of a bacterial autolytic process [58]. Tetracycline enters the cells and binds reversibly to the 30S arresting translation and thus inhibiting protein synthesis which ultimately leads to a bacteriostatic effect [59].   Sulfanilamide prevents bacterial replication by inhibiting dihydropteroate synthetase [60]. Chloramphenicol diffuses through the bacteria cell wall and reversibly bind to bacterial 50S ribosomal subunit interfering peptidyl transferase activity and block peptide bond formation impeding bacterial cell proliferation [61]. Rifampin specifically inhibits bacterial RNA polymerase arresting DNA-directed RNA synthesis of bacteria [62]. Resistance to these antibiotics may involve efflux systems that transport the antibiotics from inside to outside the bacterial cells or a ribosomal protection protein remove antibiotics from ribosomes. Resistance to rifampicin has been linked to a variety of mutations in *rpoB* and *rpoC* [63—65].

Finally, while we did not measure changes in gene expression in this study, our past study of iron (II) resistance in *E. coli* K-12 MG1655 found that there were large changes in gene expression associated with general metal resistance and iron metabolism in general [19].   We suspect that this was the case here as well and our future studies will examine this possibility.

5. Conclusions

This is the first study to utilize experimental evolution to investigate magnetite nanoparticle resistance in *E. coli* or any other bacterium.   *E. coli* K-12 MG1655 evolved resistance to magnetite nanoparticles at 25 days of selection. Resistance to magnetite nanoparticles conferred resistance to both metals and antibiotics. Increased cell length and wide resulted many have played a significant role in adaptation to magnetite. Genomic analysis revealed hard selective sweeps in the *rpoA* and *rpoC* made important contributions to magnetite nanoparticle resistance. These results have important consequences for the future use of magnetite nanoparticles as antimicrobials as de-novo evolution against these materials resulted quickly and occurred due to relatively simple genomic changes. This is an issue that will continue to be of significance regarding the use of nanomaterials as antimicrobials as we outlined in an earlier review [66].

6. Patents

N/A

Data Availability Statement:

Conflicts of Interest: The authors declare no conflict of interest.

Appendix A

Appendix A. Table A1: Operating conditions for ICP-MS determination of iron in magnetite nanoparticles

Table 1a: Parameters for microwave assisted acid digestion of samples

Digestion Parameters	Values
Power	1800 W
Temperature	190 0C
Ramp Time	25 minutes
Hold Time	20 minutes

Table 1b: Parameters for analysis of Iron by Optima 8300 ICP-OES.

ICP-OES Parameters	Values
RF Power	1500 Watts
Nebulizer	GemCone Low Flow
Nebulizer Gas Flow rate	0.80L/min
Plasma Gas Flow rate- Argon	10L/min
Sample Flow rate	1.50mL/min

Appendix A. Table A2:   Iron Concentration in bacterial samples ICP Results

Iron (II) O-hour	Theoretical Concentration (mg/L)	Measured Concentration (mg/L)	Measured Concentration (mg/L) (24hr)
	0.00	0.00	0.00
	60	12.39	17.23
	120	33.14	35.83
	250	58.89	64.01
	500	91.88	124.62
	750	169.57	181.90
	1000	226.47	215.08
	1750	371.56	328.35
	2500	424.41	180.34
	5000	1039.31	1325.78
Iron (III) O-hour			
	0	0	0.00
	60	13.10	10.70
	120	32.00	28.78
	250	71.12	58.34
	500	98.87	108.72
	750	208.18	167.00
	1000	232.15	215.97
	1750	406.15	354.42
	2500	502.55	506.06
	5000	1208.28	1897.90
Magnetite O-hour			
	0	4.25	0.00
	60	35.87	34.73
	120	81.83	65.33
	250	114.47	142.27
	500	260.86	260.11
	750	495.13	254.63
	1000	577.89	384.57
	1750	883.52	308.12
	2500	1157.75	1199.82
	5000	2474.32	2421.73
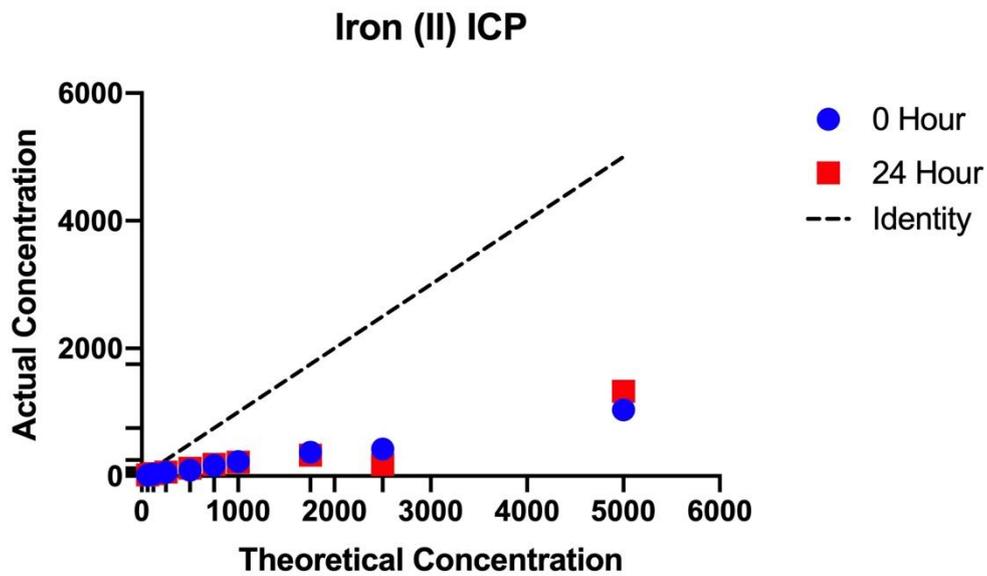
Appendix A Figure A1. This figure shows the actual amount of ionic iron (II) compared to the theoretical amount of iron (II) at 0 and 24 hours in the bacterial medium.
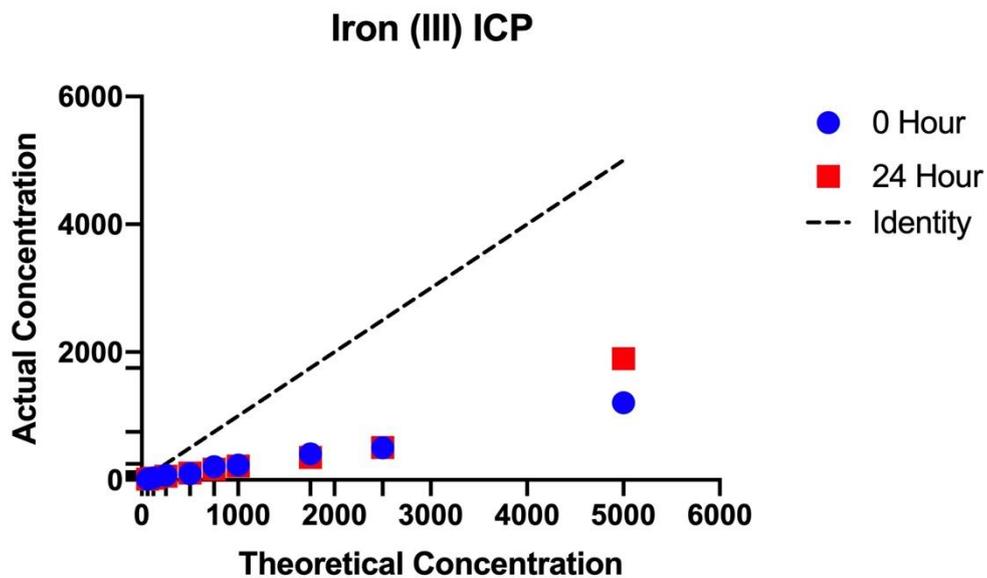
Appendix A. Figure A2. This figure shows the amount of ionic iron (III) at 0 and 24 hours resulting from iron (III) in DMB medium.
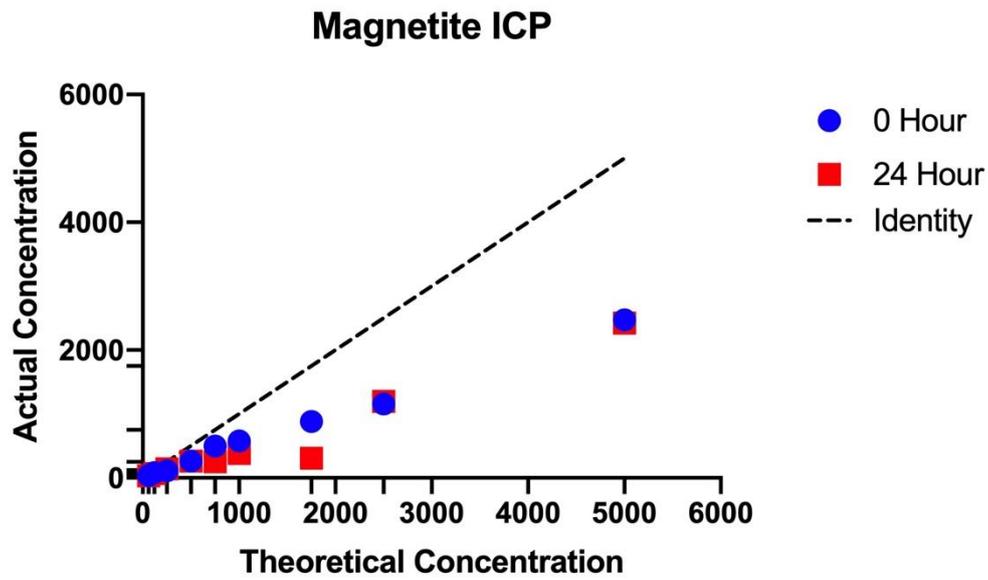
Appendix A. Figure A3.   This figure shows the amount of magnetite at 0 and 24 hours resulting from magnetite in DMB medium.

Appendix B

Table B1. Significant Polymorphisms, Control Populations, Day 28.

Gene	Mutation	Annotation	C1	C2	C3	C4	C5
ftsW →	C→T	I377I (ATC→ATT)	0.000	0.000	0.000	0.269	0.000
mhpR ←	G→A	R193C (CGC→TGC)	0.000	0.295	0.000	0.000	0.000
stfE ←	C→G	pseudogene (1/501 nt)	0.000	0.000	0.414	0.000	0.000
yddH ← / → nhoA	A→T	intergenic (-148/-25)	0.000	0.000	0.366	0.000	0.000
yejH → / → rplY	A→T	intergenic (+5/-120)	0.000	0.441	0.000	0.000	0.000
yejH → / → rplY	C→A	intergenic (+42/-83)	0.000	0.443	0.000	0.000	0.000
tktB →	C→T	P369L (CCG→CTG)	0.000	0.000	0.000	0.000	0.368
ygeY →	T→C	F233L (TTC→CTC)	0.000	0.000	0.000	0.287	0.000
xdhD →	C→T	T878M (ACG→ATG)	0.000	0.286	0.000	0.000	0.000
treF → / ← yhjB	A→G	intergenic (+14/+37)	0.000	0.000	0.000	0.000	0.303
pyrE ← / ← rph	Δ1 bp	intergenic (-41/+25)	0.250	0.000	0.000	0.000	0.429
rpoB →	C→T	H526Y (CAC→TAC)	0.000	0.000	0.000	0.540	0.000
rpoB →	C→T	S712F (TCC→TTC)	0.000	0.000	0.000	0.000	0.259
rpoB →	G→A	E848K (GAA→AAA)	0.000	0.000	0.000	0.359	0.000
rpoB →	G→T	Q1017H (CAG→CAT)	0.000	0.328	0.000	0.000	0.000
rpoC →	+TCT	coding (2012/4224 nt)	0.427	0.000	0.000	0.000	0.000

Table B2. Minor Polymorphisms, Control Populations, Day 28.

Gene	Mutation	Annotation	C1	C2	C3	C4	C5
caiT ←	A→T	N41K (AAT→AAA)	0.000	0.149	0.000	0.000	0.000
yadL ←	T→A	N179I (AAT→ATT)	0.096	0.000	0.000	0.000	0.000
afuC ←	A→G	I315T (ATA→ACA)	0.160	0.000	0.000	0.000	0.000
yagG →	G→A	S392N (AGC→AAC)	0.000	0.168	0.000	0.000	0.000
yahG →	G→A	G212R (GGA→AGA)	0.000	0.000	0.243	0.000	0.000
prpD →	G→C	T241T (ACG→ACC)	0.000	0.000	0.000	0.000	0.169
hyi →	A→T	D198V (GAT→GTT)	0.135	0.000	0.000	0.000	0.000
sfmZ ←	A→T	V50D (GTT→GAT)	0.000	0.000	0.000	0.072	0.000
nadA →	A→G	A58A (GCA→GCG)	0.000	0.236	0.000	0.000	0.000
flgE →	T→C	L325P (CTG→CCG)	0.000	0.000	0.000	0.113	0.000
nhaB ←	A→T	V475E (GTG→GAG)	0.000	0.000	0.000	0.242	0.000
sapB ←	A→G	F48S (TTT→TCT)	0.123	0.000	0.000	0.000	0.000
kilR ←	G→A	A3V (GCA→GTA)	0.000	0.000	0.000	0.000	0.179
ldhA ← / → ydbH	A→T	intergenic (-200/-8)	0.000	0.000	0.000	0.083	0.000
hipB ←	A→G	F4L (TTT→CTT)	0.119	0.000	0.000	0.000	0.000
ydfZ →	A→T	T22S (ACC→TCC)	0.000	0.000	0.000	0.160	0.000
cheW ← / ← cheA	C→T	intergenic (-18/+3)	0.000	0.000	0.000	0.000	0.236
yedQ ← / ← yodC	A→T	intergenic (-105/+66)	0.000	0.159	0.000	0.000	0.000
metG →	C→T	Q31* (CAG→TAG)	0.000	0.139	0.000	0.000	0.000
fucP →	G→A	A263A (GCG→GCA)	0.110	0.000	0.000	0.000	0.000

tcdA ← / ← mltA	T→A	intergenic (-118/+121)	0.000	0.000	0.000	0.123	0.000
ygeV ← / → ygeW	A→G	intergenic (-68/-408)	0.000	0.000	0.000	0.000	0.197
ygeV ← / → *ygeW*	G→A	intergenic (-344/-132)	0.000	0.000	0.000	0.182	0.000
serA ←	C→T	D43N (GAT→AAT)	0.000	0.160	0.000	0.000	0.000
ygiD ← / → zupT	C→G	intergenic (-39/-104)	0.000	0.000	0.000	0.000	0.098
gltB →	T→C	Y199Y (TAT→TAC)	0.136	0.000	0.000	0.000	0.000
crp →	A→T	M60L (ATG→TTG)	0.000	0.200	0.000	0.000	0.000
bcsE →	A→G	E243E (GAA→GAG)	0.000	0.000	0.000	0.094	0.000
yibG →	G→A	E28K (GAA→AAA)	0.084	0.000	0.000	0.000	0.000
metL →	C→T	A681V (GCG→GTG)	0.000	0.000	0.226	0.000	0.000

Table B3. Position and description of significant polymorphisms, Control Populations, Day 28.

Gene	Position	Description
ftsW →	99,533	lipid II flippase; integral membrane protein involved in stabilizing FstZ ring during cell division
mhpR ←	367,844	mhp operon transcriptional activator
stfE ←	1,209,619	pseudogene, e14 prophage; side tail fiber protein fragment family;Phage or Prophage Related
yddH ← / → nhoA	1,533,999	flavin reductase like-protein/N-hydroxyarylamine O-acetyl-transferase
yejH → / → rplY	2,282,397	putative ATP-dependent DNA or RNA helicase/50S ribosomal subunit protein L25
yejH → / → rplY	2,282,434	putative ATP-dependent DNA or RNA helicase/50S ribosomal subunit protein L25
tktB →	2,580,741	transketolase 2, thiamine triphosphate-binding
ygeY →	3,009,460	putative peptidase
xdhD →	3,023,948	putative hypoxanthine oxidase, molybdopterin-binding/Fe-S binding
treF → / ← yhjB	3,671,255	cytoplasmic trehalase/putative DNA-binding transcriptional response regulator

pyrE ← / ← rph	3,815,809	orotate phosphoribosyltransferase/ribonuclease PH (defective);enzyme; Degradation of RNA; RNase PH
rpoB →	4,182,820; 4,183,379; 4,183,786; 4,184, 295	RNA polymerase, beta subunit

Table B4. Position and description of minor polymorphisms, Control Populations, Day 28.

Gene	Position	Description
caiT ←	41,809	putative transporter
yadL ←	151,696	putative fimbrial-like adhesin protein
afuC ←	277,859	CP4-6 prophage; putative ferric transporter subunit
yagG →	286,569	CP4-6 prophage; putative sugar transporter
yahG →	338,958	DUF1116 family protein
prpD →	351,937	2-methylcitrate dehydratase
hyi →	536,302	hydroxypyruvate isomerase
sfmZ ←	564,332	response regulator family protein
nadA →	782,258	quinolinate synthase, subunit A
flgE →	1,133,547	flagellar hook protein
nhaB ←	1,233,294	sodium:proton antiporter
sapB ←	1,355,328	antimicrobial peptide transport ABC transporter permease
kilR ←	1,418,222	Rac prophage; inhibitor of ftsZ, killing protein
ldhA ← / → ydbH	1,443,043	fermentative D-lactate dehydrogenase, NAD-dependent/putative membrane-anchored protein, function unknown

hipB ←	1,592,433	antitoxin of HipAB toxin-antitoxin system
ydfZ →	1,629,278	selenoprotein, function unknown
cheW ← / ← *cheA*	1,973,357	purine-binding chemotaxis protein/fused chemotactic sensory histidine kinase in two-component regulatory system with CheB and CheY: sensory histidine kinase/signal sensing protein
yedQ ← / ← *yodC*	2,028,122	putative membrane-anchored diguanylate cyclase/uncharacterized protein
metG →	2,194,390	methionyl-tRNA synthetase
fucP →	2,935,023	L-fucose transporter
tcdA ← / ← *mltA*	2,945,960	tRNA threonylcarbamoyladenosine dehydratase; sulfur acceptor for CsdA/membrane-bound lytic murein transglycosylase A
ygeV ← / → *ygeW*	3,005,854; 3,006,130	putative sigma-54-interacting transcriptional activator/putative carbamoyltransferase
serA ←	3,058,284	D-3-phosphoglycerate dehydrogenase
ygiD ← / → *zupT*	3,182,446	4,5- DOPA-extradiol-dioxygenase/zinc transporter
gltB →	3,355,321	glutamate synthase, large subunit
crp →	3,486,297	cAMP-activated global transcription factor, mediator of catabolite repression
bcsE →	3,697,186	cellulose production protein
yibG →	3,768,258	TPR-like repeat protein
metL →	4,131,876	Bifunctional aspartokinase/homoserine dehydrogenase 2

References

1. He, S.; Feng, Y.; Gu, N.; Zhang, Y.; and Lin, X.; The effect of γ-Fe$_2$O$_3$ nanoparticles on *Escherichia coli* genome, *Env. Pollution* **2011,** 159: 3468—3473.

2. Hong, S.; Lu, X.; and Gao, P.; The exploration of the antibacterial mechanism of Fe^{3+} against bacteria, *Brazilian J. Microbiology* **2011**, 42: 410—414.

3. Guan, G.; Pinochet-Barros, A.; Gaballa, A.; Patel, S.J.; Argüello, J.M.; Helmann, J.D.; PfeT, a P1B4 -type ATPase, effluxes ferrous iron and protects *Bacillus subtilis* against iron intoxication, *Mol. Microbiol.* **2015**, 98(4): 787-803. doi: 10.1111/mmi.13158.

4. Fillat MF.; The FUR (ferric uptake regulator) superfamily: diversity and versatility of key transcriptional regulators. *Arch. Biochem. Biophys.* **2014**, 546: 41-52. doi: 10.1016/j.abb.2014.01.029.

5. Perez-Martin Escolar, L.; Perez-Martin, J.; and Lorenzo, V.; Opening the Iron Box: Transcriptional Metalloregulation by the Fur Protein, *J. Bacteriology*, **1999**, 181(20): p. 6223-6229.

6. Lill, R.; Function and biogenesis of iron-sulphur proteins, *Nature,* **2009**, 460(7257): 831-8. doi: 10.1038/nature08301.

7. Grass G.; Iron transport in *Escherichia coli*: All has not been said and done, *BioMetals* **2005***,* 19: 159—172. DOI: 10.1007/s10534-005-4341-2.

8. Coale, K.H.; Johnson, K.S.; Fitzwater, S.E.; Gordon, R.M.; Tanner, S.; Chavez, F.P.; Ferioli, L.; Sakamoto, C.; Rogers, P.; Millero, F.; Steinberg, P.; Nightingale, P.; Cooper, D.; Cochlan, W.P.; Landry, M.R.; Constantinou, J.; Rollwagen, G.; Trasvina, A.; Kudela, R.; A massive phytoplankton bloom induced by an ecosystem-scale iron fertilization experiment in the equatorial Pacific Ocean, *Nature* **1996**, 383 (6600):495 – 501.

9. Konopka K.; Neilands J.B.; Effect of serum albumin on siderophore-mediated utilization of transferrin iron. *Biochemistry* **1984**, 23(10):2122-7.

10. Nakashige, T.G.; Zhang, B.; Krebs, C.; Nolan, E.M.; Human calprotectin is an iron-sequestering host-defense protein, *Nat. Chem. Biol.* **2015,** 11(10): 765-71. doi: 10.1038/nchembio.1891.

11. Seo, S.W.; Kim, D.; Latif, H.; O'Brien, E.J.; Szubin, R.; Palsson, B.O.; Deciphering Fur transcriptional regulatory network highlights its complex role beyond iron metabolism in *Escherichia coli. Nat Commun.* **2014**, 5: 4910.

12. Hale, R.; Morrongiello, J.R.; Swearer, S.E.; Evolutionary traps and range shifts in a rapidly changing world. *Biol Lett.* **2016** 12(6):20160003. doi: 10.1098/rsbl.2016.0003. PMID: 27330167; PMCID: PMC4938037.

13. Thomas, M.D.; Ewunkem, A.J.; Williams, D.K.; Moore, A.; Rhinehardt, K.; Van Beveren, E.; Yang, B.; Boyd, B.; Tapia, A.; Han, J.; Harrison, S.H.; and Graves J.L. Too much of a good thing: Adaptation to iron (II) in *Escherichia coli*, *Evolution, Medicine & Public Health* **2021**, eoaa051, https://doi.org/10.1093/emph/eoaa051.

14. Graves, J.L.; Ewunkem, A.J.; Thomas, M.D.; Han, J.; Rhinehardt, K.L.; Boyd, S.; Edmondson, R.; Jeffers-Francis, L.; and Harrison, S.H. Experimental Evolution of Metal Resistance in Bacteria. In Banzhaf et al. (Eds.) *Evolution in Action—Past, Present, and Future*, pp. 91—106, (Cham, Switzerland: Springer 2 International Publishing, AG) 2020.

15. Graves J.L.; Ewunkem, J.; Ward, J.; Staley, C.; Thomas, M.D.; Rhinehardt, K.L.; Han, J.; and Harrison, S.H. Experimental evolution of gallium resistance in *Escherichia coli*, *Evolution, Medicine, and Public Health* **2019**, 10.1093/emph/eoz025.

16. Laurent, S.; Forge, D.; Port, M.; Roch, A.; Robic, C.; Vander Elst, L.; & Muller, R. N. Magnetic iron oxide nanoparticles: synthesis, stabilization, vectorization, physicochemical characterizations, and biological applications. *Chemical reviews*, **2008**, *108*(6), 2064-2110.

17. Hett, A.; *Nanotechnology: small matter, many unknowns*. Swiss Reinsurance Company, 2004.

18. Khan, I.; Saeed, K.; & Khan, I; Nanoparticles: Properties, applications and toxicities. _Arabian journal of chemistry_, **2019**, _12_(7), 908-931.

19. Niño-Martínez, N.; Salas Orozco, M. F.; Martínez-Castañón, G. A.; Torres Méndez, F.; & Ruiz, F.; Molecular mechanisms of bacterial resistance to metal and metal oxide nanoparticles. _Int. J. of Mol. Sci._ **2019**, 20(11), 2808.

20. Chamchoy, K.; Inprasit, T.; Vanichvattanadecha, C.; Thiangtrong, A.; Anukunwithaya, P.; and Pisitsak, P; The Magnetic Properties and Dye Adsorption of Sericin-modified Magnetite Nanoparticles. _J. Polymers and the Env._ **2020**, 1-8.

21. Siponen, M. I.; Legrand, P.; Widdrat, M.; Jones, S. R.; Zhang, W. J.; Chang, M. C.; Faivre, D; Arnoux, P.; & Pignol, D; Structural insight into magnetochrome-mediated magnetite biomineralization. _Nature_, **2013**, 502(7473), 681-684.

22. Gieré, R.; Magnetite in the human body: Biogenic vs. anthropogenic. _Proc. Nat. Acad. Sci. USA._ **2016**, 113(43), 11986-11987.

23. Peters, S. T.; Alibabaie, N.; Pack, A.; McKibbin, S. J.; Raeisi, D.; Nayebi, N.; Torab, F.; Ireland, T; & Lehmann, B.; Triple oxygen isotope variations in magnetite from iron-oxide deposits, central Iran, record magmatic fluid interaction with evaporite and carbonate host rocks. _Geology_ **2019**, 48(3), 211-215.

24. Ayupova, N. R.; Novoselov, K. A.; Maslennikov, V. V.; Melekestseva, I. Y.; Hollis, S. P.; Artemyev, D. A.; & Tessalina, S. G.; The formation of magnetite ores of the Glubochenskoe deposit, Turgai iron belt, Russia: new structural, mineralogical, geochemical, and isotopic constraints. _Mineralium Deposita_ **2020**, 1-21.

25. Kirschvink, J. L.; Kobayashi-Kirschvink, A.; & Woodford, B. J.; Magnetite biomineralization in the human brain. _Proc. Nat. Acad. Sci. USA_ **1992**, 89(16), 7683-7687.

26. Kim, D. H.; Nikles, D. E.; & Brazel, C. S.; Synthesis and characterization of multifunctional chitosan-$MnFe_2O_4$ nanoparticles for magnetic hyperthermia and drug delivery. Materials **2010**, 3(7), 4051-4065.

27. Alvarez-Berríos, M. P.; Castillo, A.; Rinaldi, C.; & Torres-Lugo, M.; Magnetic fluid hyperthermia enhances cytotoxicity of bortezomib in sensitive and resistant cancer cell lines. _Int. J. Nanomedicine_ **2014**, 9, 145.

28. Tokajuk, G.; Niemirowicz, K.; Deptuła, P.; Piktel, E.; Cieśluk, M.; Wilczewska, A. Z.; Dąbrowski, J.R.; & Bucki, R.; Use of magnetic nanoparticles as a drug delivery system to improve chlorhexidine antimicrobial activity. _International Journal of Nanomedicine_ **2017**, _12_, 7833.

29. de Toledo, L. D. A. S.; Rosseto, H. C.; & Bruschi, M. L.; Iron oxide magnetic nanoparticles as antimicrobials for therapeutics. Pharma. Develop. and Tech. **2018**, 23(4), 316-323.

30. Wang, J.; Wu, H.; Yang, Y.; Yan, R.; Zhao, Y.; Wang, Y.; Chen A.; Shao, S.; Jiang, P.; & Li, Y; Bacterial species-identifiable magnetic nanosystems for early sepsis diagnosis and extracorporeal photodynamic blood disinfection. _Nanoscale_ **2018**, _10_(1), 132-141.

31. Iqbal, J.; Abbasi, B. A.; Ahmad, R.; Shahbaz, A.; Zahra, S. A.; Kanwal, S.; Kanwal, S.; Munir, A.; Rabbani, A.; & Mahmood, T.; Biogenic synthesis of green and cost-effective iron nanoparticles and evaluation of their potential biomedical properties. _J. Mol. Structure_ **2020**, 1199: 126979.

32. Taimoory, S. M.; Rahdar, A.; Aliahmad, M.; Sadeghfar, F.; Hajinezhad, M. R.; Jahantigh, M.; Shahbazi, P.; & Trant, J. F.; The synthesis and characterization of a magnetite nanoparticle with potent antibacterial activity and low mammalian toxicity. _J. Mol. Liquids_ **2018**, 265, 96-104.

33. Oliveira, A. M. D.; Mateus, G. A. P.; Santos, T. R. T. D.; Filho, B. A. D. A.; Gomes, R. G.; & Bergamasco, R.;; Functionalized magnetite nanoparticles with *Moringa oleifera* with potent antibacterial action in wastewater. *Environmental Technology* **2020**, 1-10.

34. Ismail, R. A.; Sulaiman, G. M.; Abdulrahman, S. A.; & Marzoog, T. R.; Antibacterial activity of magnetic iron oxide nanoparticles synthesized by laser ablation in liquid. *Mat. Sci. Eng. C* **2015**, 53, 286-297.

35. Wilczewska, A. Z.; Niemirowicz, K.; Markiewicz, K. H.; & Car, H.; Nanoparticles as drug delivery systems. *Pharma. Reports* **2012**, 64(5), 1020-1037.

36. Gabrielyan, L.; Hakobyan, L.; Hovhannisyan, A.; & Trchounian, A.; Effects of iron oxide (Fe_3O_4) nanoparticles on *Escherichia coli* antibiotic-resistant strains. *J. App. Micro.* **2019**, *126*(4), 1108-1116.

37. International Organization for Standardization.; Clinical Laboratory Testing and in Vitro Diagnostic Test Systems-Susceptibility Testing of Infectious Agents and Evaluation of Performance of Antimicrobial Susceptibility Test Devices: Reference Method for Testing the in Vitro Activity of Antimicrobial Agents Against Rapidly Growing Aerobic Bacteria Involved in Infectious Diseases. ISO, 2006.

38. Mabrouk, M.; Abd El-Wahab, R. M.; Beherei, H. H.; Selim, M. M.; & Das, D. B.; Multifunctional magnetite nanoparticles for drug delivery: Preparation, characterization, antibacterial properties and drug release kinetics. *Int. J. Pharmaceutics* **2020**, *587*, 119658.

39. Deatherage, D.E.; & Barrick, J.E.; Identification of mutations in laboratory-evolved microbes from next-generation sequencing data using breseq. *Methods Mol. Biol.* **2014**, 1151: 165-88. doi: 10.1007/978-1-4939-0554-6_12.

40. Cao, J.; Woodhall, M.R.; Alvarez, J.; Cartron, M.L.; & Andrews, S.C.; EfeUOB (YcdNOB) is a tripartite, acid-induced and CpxAR-regulated, low-pH Fe^{2+} transporter that is cryptic in *Escherichia coli* K-12 but functional in *E. coli* O157:H7. *Mol. Microbiol.* **2007**, 65(4): p. 857-75.

41. Graves Jr, J. L.;Tajkarimi, M.; Cunningham, Q.; Campbell, A.; Nonga, H.; Harrison, S. H.; & Barrick, J. E.; Rapid evolution of silver nanoparticle resistance in *Escherichia coli. Frontiers in genetics* **2015**, *6*:42 doi: 10.3389/fgene.2015.00042. PMID: 25741363; PMCID: PMC4330922.

42. Tajkarimi, M.; Rhinehardt, K.; Thomas, M.; Ewunkem, J.A.; Campbell, A.; Boyd, S.; Turner, D.; Harrison, S.H.; & Graves, J.L.; Selection for ionic- confers silver nanoparticle resistance in *Escherichia coli*. JSM *Nanotechnology and Nanomedicine* **2017**, 5: 1047.

43. Kenzaka, T.; & Tani, K.; Scanning electron microscopy imaging of bacteria based on nucleic acid sequences. In *Scanning Electron Microscopy*. Intech Open, 2012.

44. Barber, D.S.; Denslow, N.D.; Griffitt, R.J.; Martyniuk, C.J.; Sources, fate, and effects of engineered nanomaterials in the aquatic environment, in Sahu SC. and Casciano DA (Eds.) *Nanotoxicity: From In Vivo and In Vitro models to Health Risks,* (West Sussex, UK: Wiley), 2009.

45. Wu, H.; Yin, J. J.; Wamer, W. G.; Zeng, M.; & Lo, Y. M.; Reactive oxygen species-related activities of nano-iron metal and nano-iron oxides. *J. Food and Drug Anal.* **2014**, 22(1), 86-94.

46. Rajab, S.; Tabandeh, F.; Shahraky, M.K.; & Alahyaribeik, S.; The effect of lactobacillus cell size on its probiotic characteristics. *Anaerobe.* **2020** 62: 102103. doi: 10.1016/j.anaerobe.2019.102103. Epub 2019 Sep 13. PMID: 31525452.

47. Vijay, S.; Vinh, D.N.; Hai, H.T.; Ha,V.T.N.; Dung V.T.M.; Dinh, T.D.; Nhung, H.N.; Tram, T.T.B.; Aldridge, B.B.; Hanh, N.T.; Thu, D.D.A.; Phu, N.H.; Thwaites, G.E.; Thuong, N.T.T.; Influence of stress and antibiotic resistance on cell-length distribution in *Mycobacterium tuberculosis* clinical isolates. *Front. Microbiol.* **2017**; 8:2296. doi: 10.3389/fmicb.2017.02296. PMID: 29209302; PMCID: PMC5702322.

48. Manina, G.; Dhar, N.; & McKinney, J. D.; Stress and host immunity amplify *Mycobacterium tuberculosis* phenotypic heterogeneity and induce nongrowing metabolically active forms. *Cell host & microbe* **2015**, 17(1), 32-46.

49. Priestman, M.; Thomas, P.; Robertson, B. D.; & Shahrezaei, V.; *Mycobacteria* modify their cell size control under sub-optimal carbon sources. *Frontiers in cell and developmental biology* **2017**, *5*: 64.

50. Justice, S. S.; Hunstad, D. A.; Cegelski, L.; & Hultgren, S. J.; Morphological plasticity as a bacterial survival strategy. *Nat. Reviews Micro.* **2008**, 6(2), 162-168.

51. Koch, A.; Mizrahi, V.; & Warner, D. F.; The impact of drug resistance on *Mycobacterium* tuberculosis physiology: what can we learn from rifampicin? *Emerging microbes & infections* **2014**, *3*(1), 1-11.

52. Monds, R. D.; Lee, T. K.; Colavin, A.; Ursell, T.; Quan, S.; Cooper, T. F.; & Huang, K. C.; Systematic perturbation of cytoskeletal function reveals a linear scaling relationship between cell geometry and fitness. *Cell Reports* **2014**, 9(4): 1528-1537.

53. Bos, J.; Zhang, Q.; Vyawahare, S.; Rogers, E.; Rosenberg, S. M.; & Austin, R. H.; Emergence of antibiotic resistance from multinucleated bacterial filaments. *Proc. Nat. Acad. Sci. USA* **2015**, *112*(1), 178-183.

54. Rodríguez-Verdugo, A.; Carrillo-Cisneros, D.; González-González, A.; Gaut B.S.; & Bennett, A.F. Different tradeoffs result from alternate genetic adaptations to a common environment. *Proc. Natl. Acad. Sci. U S A.* **2014**, 111(33):12121-6. doi: 10.1073/pnas.1406886111. PMID: 25092325; PMCID: PMC4143048.

55. Cheng, K. K.; Lee, B. S.; Masuda, T.; Ito, T.; Ikeda, K.; Hirayama, A., Deng, L.; Dong, J.; Shimizu, K.; Soga, T.; Tomita, M.; Palsson, B.O.; & Tomita, M.; Global metabolic network reorganization by adaptive mutations allows fast growth of *Escherichia coli* on glycerol. *Nat. Comm.* **2014**, 5(1), 1-9.

56. Petcharoen, K.; & Sirivat, A.; Synthesis and characterization of magnetite nanoparticles via the chemical co-precipitation method. *Mat. Sci. Eng.* B **2012**, 177(5), 421-427.

57. Wei, L.; Lu, J.; Xu, H.; Patel, A.; Chen, Z. S.; & Chen, G.; Silver nanoparticles: synthesis, properties, and therapeutic applications. *Drug Discovery Today* **2015**, 20(5), 595-601.

58. Kaushik, D.; Mohan, M.; Bora De, D. M.; & Swami, O. C.; Ampicillin: rise fall and resurgence. *JCDR* **2014**, 8(5), ME01.

59. Grossman, T. H.; Tetracycline antibiotics and resistance. *Cold Spr. Harbor Pers. Med.* **2016**, 6(4), a025387.

60. Samigulina, G. A.; & Samigulina, Z. I.; Drag design of sulfanilamide based on the technology of immune network modeling and ontological approach. In 2016 IEEE 10th International Conference on Application of Information and Communication Technologies **2016**, (AICT) (pp. 1-5). IEEE.

61. Chandrasekaran, K.; Varaprasad, K.; Venugopal, S. K.; Arun, L.; & Hameed, A. S. H.; Synergistic antibacterial effect of the magnesium-doped ZnO nanoparticles with chloramphenicol. *BioNanoScience* **2019**, 1-6.

62. Somoskovi, A.; Parsons, L. M.; & Salfinger, M.; The molecular basis of resistance to isoniazid, rifampin, and pyrazinamide in *Mycobacterium tuberculosis*. *Respiratory Research* **2001**, 2(3), 164.

63. White-Ziegler, C. A.; Um, S.; Perez, N. M.; Berns, A. L.; Malhowski, A. J.; & Young, S.; Low temperature (23 C) increases expression of biofilm-, cold-shock- and RpoS-dependent genes in *Escherichia coli* K-12. *Microbiology* **2008**, 154(1), 148-166.

64. Zaw, M.T.; Emran, N.A.; Lin, Z.; Mutations inside rifampicin-resistance determining region of *rpoB* gene associated with rifampicin-resistance in *Mycobacterium tuberculosis*. *J Infect Public Health*. **2018** 11(5): 605-610. doi: 10.1016/j.jiph.2018.04.005. PMID: 29706316.

65. Knöppel, A.; Näsvall, J.; & Andersson, D. I.; Evolution of antibiotic resistance without antibiotic exposure. *Antimicrobial Agents and Chemotherapy* **2017**, 61(11).

66. Graves, J.L.; Thomas, M.; Ewunkem, J.A.; Antimicrobial Nanomaterials: Why Evolution Matters. *Nanomaterials* (Basel). **2017**, 7(10):283. doi: 10.3390/nano7100283. PMID: 28934114; PMCID: PMC5666448.